NANO LETTERS

Letter

pubs.acs.org/NanoLett

High-Performance, Transparent, and Stretchable Electrodes Using Graphene–Metal Nanowire Hybrid Structures

Mi-Sun Lee,[†] Kyongsoo Lee,[†] So-Yun Kim,[†] Heejoo Lee,[†] Jihun Park,[†] Kwang-Hyuk Choi,[‡] Han-Ki Kim,[‡] Dae-Gon Kim,[§] Dae-Young Lee,[∥] SungWoo Nam,[#] and Jang-Ung Park*[,†]

[†]School of Nano-Bioscience and Chemical Engineering, School of Mechanical and Advanced Materials Engineering, Low-Dimensional Carbon Materials Center, Ulsan National Institute of Science and Technology (UNIST), Ulsan, 689-798, Republic of Korea

[‡]Department of Advanced Materials Engineering for Information and Electronics, Kyung Hee University, Yongin-si, 446-701, Republic of Korea

[§]Samsung Techwin R&D Center, Seongnam-si, 463-400, Republic of Korea

[∥]Display Research Center, Samsung Display, Yongin-city, 446-711, Republic of Korea

[#]Department of Mechanical Science and Engineering, University of Illinois at Urbana–Champaign, Urbana, Illinois 61801, United States

Supporting Information

ABSTRACT: Transparent electrodes that can remain electrically conductive and stable under large mechanical deformations are highly desirable for applications in flexible and wearable electronics. This paper describes a comprehensive study of the electrical, optical, and mechanical properties of hybrid nanostructures based on two-dimensional graphene and networks of one-dimensional metal nanowires, and their use as transparent and stretchable electrodes. Low sheet resistance (33 Ω/sq) with high transmittance (94% in visible range), robust stability against electric breakdown and oxidation, and superb flexibility (27% in bending strain) and stretchability (100% in tensile strain) are observed, and these multiple functionalities of the hybrid structures suggest a future promise for next generation electronics. The use of hybrid electrodes to fabricate oxide semiconductor transistors and single-pixel displays integrated on wearable soft contact lenses with in vivo tests are demonstrated.

KEYWORDS: *Nanowires, graphene, hybrid, transparent electrodes, stretchable electronics*

Transparent electrodes have been widely used in electronics such as displays, touch screens, solar cells, and light-emitting devices. Recently, encoding mechanical flexibility and stretchability into transparent electrodes has been extensively explored as the key in emerging flexible electronics. Although indium tin oxide (ITO) is the most commonly used material for transparent electrodes, its brittleness and growing cost of indium limit its utility for flexible devices. Thus, there is a clear and urgent need for new transparent conductive materials with superb mechanical properties. Several alternative materials to ITO, including conductive polymers,[1] carbon nanotubes,[1−5] graphene,[6−16] nanowires,[2,17−26] and metal mesh-structures,[15,26−28] have been studied for this purpose. Among these alternatives, two-dimensional graphene and percolating networks of one-dimensional metal nanowires (mNWs) have been considered as promising candidates for next-generation transparent electrodes, due to their high mechanical flexibility as well as good optical transparency and electric conductivity. For example, monolayer graphene can be distorted up to a strain of ∼4% with negligible cracking[14] and absorbs only 2.3% of visible light.[7] In addition, the theoretical minimum sheet resistance (R_s) of pristine graphene has been estimated to be as low as ∼30 Ω/sq.[8] However, scalable graphene synthesis methods such as epitaxially grown graphene on silicon carbide[9] and chemical vapor deposited (CVD) graphene on Ni or Cu catalysts[6,10−12] produce relatively lower quality graphene with polycrystalline structures and defects (i.e., grain boundaries, ripples, wrinkles, folds, cracks, etc.), and hence the experimental R_s of the undoped, synthesized graphene (≥∼ 1 kΩ/sq)[6,11−13] is significantly higher than R_s of ITO (<∼ 80 Ω/sq with transmittance of ∼90% at 550 nm).[15] Although chemical doping methods[14,16] can further reduce R_s of the CVD synthesized graphene by increasing carrier density, instability of the graphene–dopant interactions in air and under thermal loading typically limits the lifetime of this doping effect and causes a time-variant increase of R_s.[15]

Instead, another promising alternative to ITO is the networks of randomly distributed mNWs.[21−25] Charge transport occurs along the NWs, and open spaces between NWs provide optical transparency. Typically, R_s of the mNW

Received: March 24, 2013
Revised: May 7, 2013
Published: May 23, 2013

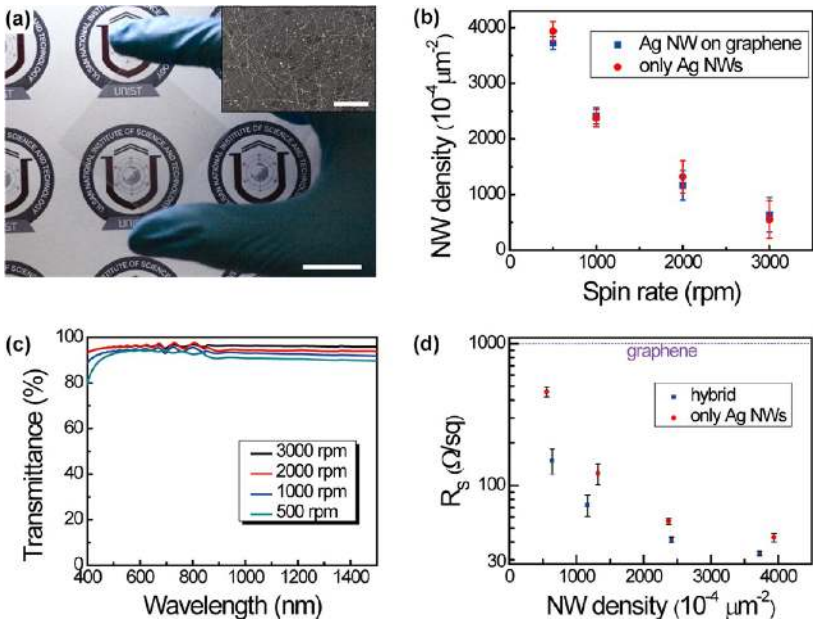

Figure 1. Fabrication and quantitative analysis of graphene−AgNW hybrid nanostructures. (a) Photograph of graphene−AgNW hybrid film on a PET substrate. The scale bar indicates 2 cm. The inset shows a SEM image of this hybrid (scale bar, 5 μm). (b) Dependence of AgNW density (in the area of 100 × 100 μm^2) on spin rate. (c) Optical transmittance spectra of the hybrid films where AgNWs are coated with different spin rates. (d) Log-scale plots of the sheet resistances as a function of NW density.

networks (<∼ 80 Ω/sq)[21−23] for transmittance of >90% are lower than the R_s of the undoped, CVD synthesized graphene, and comparable with that of ITO. Also, their mesh-like geometries present outstanding mechanical robustness when bent (up to a strain of ∼1%)[21,22] or stretched (over a strain of ∼50%).[24,25] The mNWs are normally coated as networks by solution processes, which can facilitate the low-cost, high-speed fabrication of transparent electrodes. However, disadvantages of the mNW networks, such as (i) low breakdown voltages, (ii) typically high NW−NW junction resistance, (iii) high contact resistance between the network and active materials due to the noncontacted, open spaces within the network, (iv) material instability in harsh environment, and (v) their poor adhesion to plastic substrates, have limited their integration into commercial devices.[19,21−26]

Here, we report graphene-mNW hybrid structures as high-performance, transparent, and stretchable electrodes. The graphene-mNW hybrid films have been recently explored but only for the subpercolation regime, where NWs with low densities below the percolation threshold cannot form their own conductive paths but can locally improve the conductivity of graphene by providing conductive pathways through defects of polycrystalline graphene.[29−31] In our approach, percolating networks of mNWs with high densities above the percolation threshold were integrated into graphene, without significant reduction of transmittance. Here, both conducting components of graphene and the mNW percolating network allow simultaneous charge transport in the hybrid nanostructure, each complementing the disadvantages of the other component. This hybrid structure can reduce R_s down to ∼33 Ω/sq for a transmittance of 94%, while preserving these electrical and optical properties reliably against thermal oxidation conditions (85% in humidity, 85 °C, 240 h), and also present superb mechanical flexibility (folding with minimum bending radius of ∼3.7 μm) and stretchability (maximum stretching strain of 100%). Compared to the single material of graphene or mNW network, the formation of this hybrid can significantly improve robustness against an electrical breakdown as well, which suggests its potential advantages for highly integrated and miniaturized devices. This hybrid nanostructure is transferable onto a variety of substrates, including soft eye contact lenses. Inorganic light-emitting diode (ILED) devices fitted on a soft eye contact lens using the transparent, stretchable interconnects of the hybrid electrodes demonstrate an application example toward flexible and wearable electronics. Furthermore, oxide semiconductor transistor arrays with source/drain electrodes of the hybrid structure suggest the future promise for the integration into commercial devices.

The hybrid transparent conductive film can be fabricated by spinning a suspension of Ag nanowires (AgNWs) onto a CVD-synthesized graphene layer, and AgNWs are attached to graphene through van der Waals force (see Supporting Information). Figure 1a presents a photo and SEM image of the graphene−AgNW hybrid film on a PET substrate. As shown in the AFM image of Figure S2a, the average diameter and length of the AgNWs are 20 nm and 30 μm, respectively. The average density of the NWs coated on the graphene surface is controlled within the range between 640 ± 300 and 3730 ± 114 NWs per 100 × 100 μm^2 area (Figure 1b) using different spin rates. Lower spin rates result in smaller deviations of the NW density and better uniformity (Supporting Table 1), which causes smaller deviations of sheet resistance values (Figure 1d). These densities belong to the percolation regime. For example, conductive paths along solely AgNWs are yielded when the NWs with the similar density range are coated on the PET with no graphene. Figure 1c plots the transmittances for the graphene−AgNW hybrid films with several different NW densities. These transmittances are higher than 94% in the visible range and almost consistent in the broad range from 400 to 1500 nm. Unlike the single material of graphene or AgNWs, only ∼2−3% loss of transmittance is introduced by forming the hybrid structure (Figure S2b). This high transparency of the

dx.doi.org/10.1021/nl401070p | Nano Lett. 2013, 13, 2814−2821

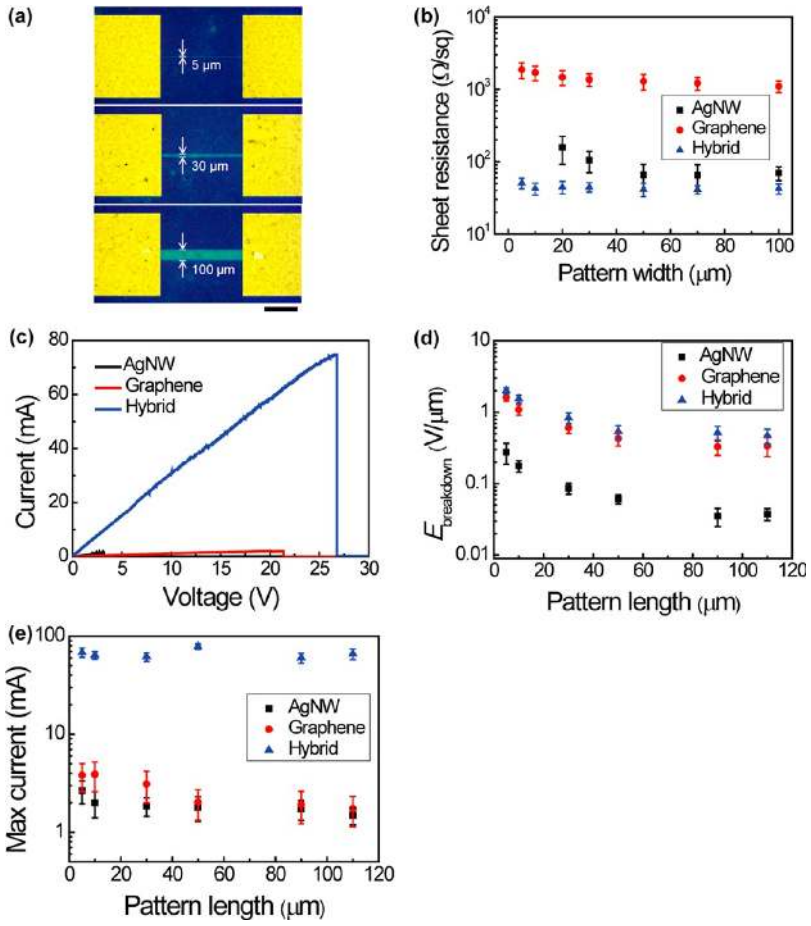

Figure 2. Electrical properties of the hybrid patterns. (a) Optical images of graphene–AgNW hybrid electrodes with different pattern widths. The scale bar is 200 μm. (b) Dependence of sheet resistance on the width of patterns (pattern length: 500 μm). The *Y*-axis in the graph is plotted on a logarithmic scale. (c) *I*–*V* characteristics of AgNWs, graphene, and their hybrid patterns (pattern width: 10 μm, length: 50 μm). (d) Dependence of the breakdown electric fields on the length of patterns (pattern width: 10 μm). The *Y*-axis in the graph is plotted on a logarithmic scale. (e) Log-scale plots of the max current versus pattern length for these three materials (pattern width: 10 μm).

hybrid in the visible light is comparable to ITO, and their transmittances in the near-infrared region are superior than ITO that has strong absorption for wavelengths over 1100 nm.[22] As shown in Figure 1d, the R_s of the hybrid film can be reduced with increasing the density of AgNWs via the modulation of the spin rate, and the lowest R_s of 33 Ω/sq with the transmittance of 94% (at 550 nm) was achieved. This R_s is significantly lower than that of the CVD graphene ($R_s \geq \sim$ 1 kΩ/sq) and comparable to the ITO electrode.

We compared the resistance of this hybrid nanostructure ($R_{s,hybrid}$) to the case where two singular components of graphene and AgNWs are connected as resistors in parallel without forming the hybrid geometry (Figure S2c). Sheet resistance in this parallel circuit ($R_{s,parallel}$) can be calculated, according to $1/R_{s,parallel} = 1/R_{s,graphene} + 1/R_{s,AgNW}$. For this calculation, $R_{s,graphene}$ (1.02 kΩ/sq) and $R_{s,AgNW}$ were experimentally measured after producing graphene and AgNW networks separately. Figure S2c indicates $R_{s,hybrid}$ is lower than $R_{s,parallel}$ overall, which means two components of the graphene and AgNWs in the hybrid form do not provide independent pathways for carriers but improve their own conductances complementarily. For example, the AgNW bridges across defects of the polycrystalline graphene can reduce the resistance of graphene significantly,[29−31] and graphene occupying empty spaces of the AgNW network also can improve the conductance. The relative difference in R_s values of the parallel circuit model and the hybrid electrode can fall below 20%, which indicates that the dense network of AgNWs becomes the main conductive component and graphene acts as an additional component, as the density of AgNWs increases (Figure S2d).

Electrical properties can be changed by pattern geometries. For this study, we photolithographically patterned the three materials (graphene, AgNWs, and the hybrid) with various widths and lengths using oxygen plasma exposure and wet etching (see Supporting Information and Figure 2a), and then measured their resistances to compare the R_s after depositing two contact pads of metals (2 nm thick Cr and 300 nm thick Au). As shown in Figure 2b, R_s of the AgNW network shows a large variation by changing widths of patterns because locally disconnected areas are produced by etching NWs. In contrast to a 2D graphene layer that presents negligible dependence of R_s on the pattern width, for example, R_s of the AgNW network increases significantly as the width decreases to the level similar to the NW length (~30 μm) and becomes nonconductive for the width less than 20 μm (at the case of 500 μm in pattern length). In addition, the R_s dependent on the width can vary by changing the pattern length as well (Figure S4). For example, the narrow widths below 20 μm can be conductive for short lengths of patterns (length < 100 μm). This R_s dependence on width and length can yield undesirable, local changes in

dx.doi.org/10.1021/nl401070p | *Nano Lett.* 2013, 13, 2814–2821

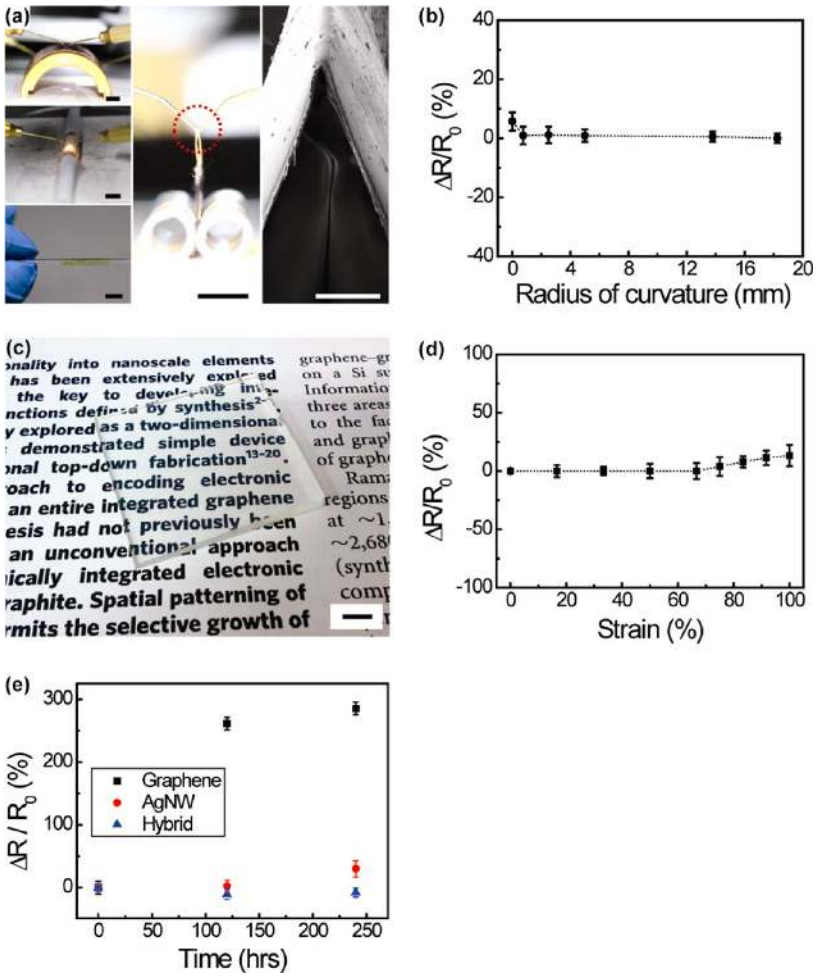

Figure 3. Mechanical properties and reliability of the hybrid nanostructures. (a) Photos of the hybrid electrodes wrapped on various cylindrical supports with different curvatures. In the middle and right parts of (a), are a photo and SEM image of the hybrid sample folded in half (radius of curvature: ~3.7 μm), respectively. Black scale bar, 5 mm. White scale bar, 50 μm. (b) Relative difference in resistance as a function of radius of curvature. (c) A photograph of the hybrid film on a PDMS substrate which is rested on a paper. Scale bar, 5 mm. (d) Relative change in the resistance as a function of tensile strain. (e) Plot of the sheet resistance versus time for graphene, AgNWs, and their hybrid films after exposure to humid and hot air (temperature: 85 °C, humidity: 85%) for 240 h.

resistance of circuits, and hence can limit the use of AgNWs for designing compactly integrated circuits that require diverse and fine electrode geometries. On the other hand, the graphene–AgNW hybrid electrode presents negligible dependence of R_s on pattern structures similar to graphene but preserves significantly lower R_s even for narrow patterns below 20 μm in width (Figure 2b). These sizes (5–20 μm in width) are comparable to the dimensions of electrodes for recent displays and touch-screen panels. This consistency in R_s and high conductance are advantages of the hybrid electrode.

In addition, the robustness of conductive materials that can withstand electrical load becomes one of important features, as devices are highly integrated and miniaturized. The I–V characteristics of graphene, AgNWs, and the hybrid with various lengths (L) of patterns were measured in ambient air. As an example, Figure 2c presents breakdown behaviors of the three materials for a 50 μm-long and 10 μm-wide pattern. The slopes in the I–V curves indicate conductances, and the narrow pattern size caused the relatively large resistance (~2 kΩ) of AgNW networks, compared to resistance of the hybrid, because only small portions of conductive pathways along the NWs remained inside the patterns. For all of the three, currents increase almost linearly with the applied bias before their breakdowns. Figure 2d compares the breakdown electric fields ($E_{breakdown}$) from various L of these three different materials. In the case of AgNW network that can be degraded by electromigration,[32] the breakdown occurs at a relatively low bias ($E_{breakdown}$ < 0.1 V/μm) for $L \geq \sim 30$ μm (average length of AgNWs), due to the large aspect ratio of NWs and NW–NW contact resistances. This $E_{breakdown}$ increases with reducing L below 30 μm, because more NWs can bridge two metal contact pads directly without NW–NW junctions. On the other hand, the $E_{breakdown}$ of CVD graphene is bigger about 10-fold compared to the AgNW network, as shown in Figure 2d. This polycrystalline graphene can be damaged by Joule heating and oxidation at the defect sites,[33] and the $E_{breakdown}$ of graphene also increases when L falls below the threshold related to grain sizes. In the graphene–AgNW hybrid nanostructure, graphene underneath AgNWs can create a path to dissipate heat and electric stress, which can make AgNWs sustainable against breakdown at relatively high electric fields. Therefore the hybrid exhibits the highest values of $E_{breakdown}$ among the three materials (graphene, AgNW networks, and the hybrid). Also, the hybrid electrode can

dx.doi.org/10.1021/nl401070p | Nano Lett. 2013, 13, 2814–2821

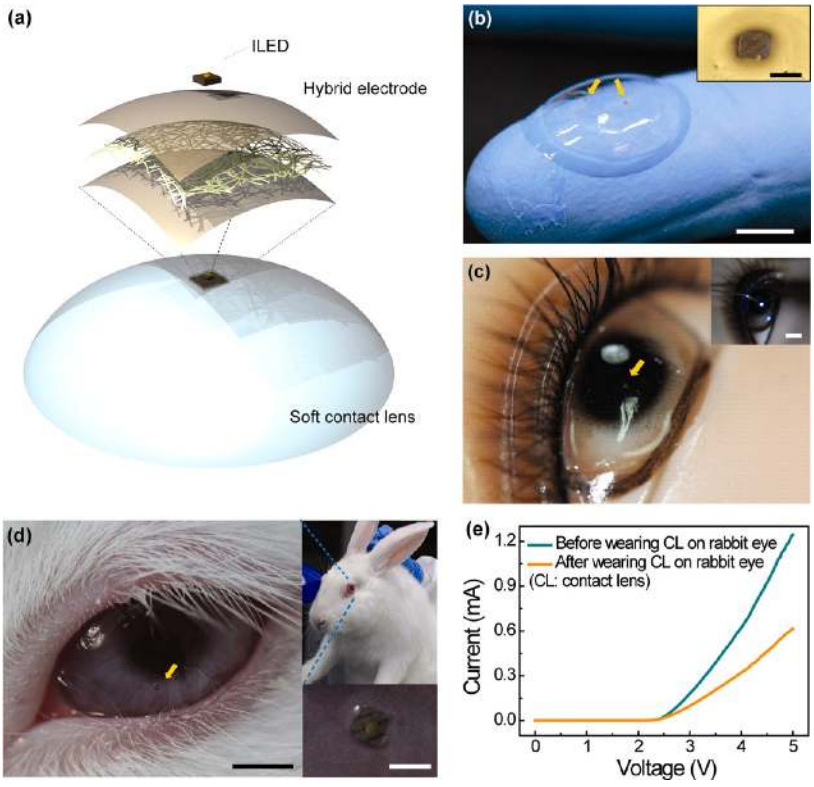

Figure 4. Single-pixel contact lens display fabricated using an inorganic light-emitting diode and the hybrid electrode. (a) Schematic illustration of the device layout. (b) A photograph of the contact lens device. Scale bar, 5 mm. (Inset: optical microscopic image of slightly sunken ILED on the surface of hybrid electrode and contact lens. Scale bar, 300 μm). (c) A photograph of the ILED-hybrid electrode-contact lens device on an eye of a mannequin. Scale bar, 5 mm. (Inset: a photograph for emitting light of contact lens device on a mannequin eye after supplying bias. Scale, 5 mm.). (d) A photograph of contact lens device on a rabbit eye and magnified image of ILED part of the device (right-bottom inset). Black scale bar, 5 mm. White scale bar, 300 μm. (e) $I-V$ characteristic curve of ILED before and after wearing contact lens device on a rabbit eye.

flow the highest current against its breakdown due to its low resistance, as shown in Figure 2e. This improved robustness of the hybrid against electrical load is another advantage.

Flexible and stretchable electronics represents an important application area that can take advantage of the graphene–AgNW hybrid nanostructures. We demonstrate the ultimate flexibility (folding capability) of the hybrid electrode in Figure 3. To realize this, a CVD graphene layer was transferred onto a 2 μm thick polyimide substrate, followed by spin-coating of AgNWs (see Supporting Information). As shown in Figure 3a, the hybrid electrodes were wrapped on various cylindrical supports with different curvatures, and folded in half by pressing two pieces of Si wafer using tape to attach both ends of the polyimide to the wafer. The right inset presents a SEM image of the folded area (radius of curvature: ~3.7 μm). Figure 3b shows the relative difference in R_s as a function of bending-induced strain (ε).[6,14] Although this folding leads to a strain of ~27%, no significant change in R_s occurs for the bending to radii of curvature as small as 3.7 μm. In addition, the large elasticity of graphene[34] and the mesh geometry of AgNW networks[24,25,35] enable the hybrid electrodes to be stretchable mechanically with preserving electric resistance. For the measurement of the stretchable characteristics of the hybrid, a PDMS elastomeric substrate was used instead of the polyimide. Figure 3c presents a photograph of the hybrid film on PDMS which is rested on a paper to demonstrate its transparent properties. After clamping this conductive sample by two fixtures connected to the current–voltage measurement system, it was stretched to specific elongation lengths using a mechanical apparatus. Figure 3d shows the relative change in the resistance under various tensile strains, and the hybrid electrode can be stretched up to 100% tensile strain with negligible resistance change. This mechanical stability of the hybrid nanostructure against bending and stretching is superior compared to ITO that can be cracked by applying a bending or tensile strain of ~1%.

Furthermore, we tested thermal oxidation stabilities of graphene, AgNWs, and the hybrid. For this test, the hybrid film was formed by transferring the graphene onto a PET film where AgNWs were precoated, and then exposed to the condition at 85 °C and 85% RH for 240 h. It has been known that AgNWs are oxidized when it is exposed to air.[22,23,26] X-ray diffraction (XRD) and energy dispersive spectroscopy (EDS) measurements of the AgNW film clearly confirms the formation of silver oxides after the thermal oxidation stability test (Figure S5). The formation of silver oxide on the surface of AgNW increases the contact resistance among NWs, which results in increasing R_s of AgNW networks (Figure 3e). In contrast, the graphene–AgNW hybrid film exhibits negligible change in R_s because oxygen gas and moisture cannot permeate through the graphene layer consistent with previous literature.[36,37] Here the graphene covering AgNWs can act as a passivation layer to retard Ag oxidation as well as providing conductive paths.

As a demonstration of device fabrication using the hybrid electrodes, a single-pixel contact lens display was fabricated by integrating an inorganic light-emitting diode (ILED) on a soft eye contact lens with the flexible and stretchable interconnects of the graphene–AgNW hybrid. The fundamental goal of this

dx.doi.org/10.1021/nl401070p | *Nano Lett.* 2013, 13, 2814–2821

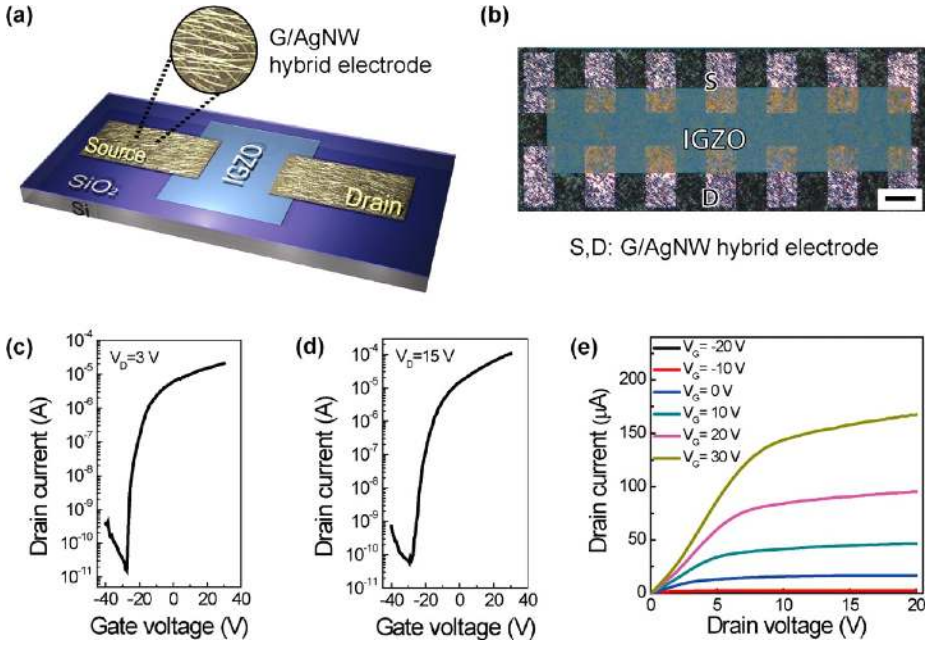

Figure 5. Oxide semiconductor transistors with source/drain electrodes of graphene–AgNW hybrid. (a) Schematic illustration of the transistor layout. (b) Optical micrograph (top-view) of the transistor. Scale bar, 100 μm. Transfer (I_d–V_g) characteristics of the transistor in (c) the linear (V_d: 3 V) and (d) saturation regimes (V_d: 15 V). (e) Output (I_d–V_d) characteristics.

future display is to create see-through contact lens devices that can overlay visual information on the real world, providing immediate, hands-free access to information.[38−40] Here, an important challenge is the safe operation of this display on a live eye, and hence it is necessary to adapt the devices to wearable contact lenses, including hydrogel-type soft lenses, instead of to lens-shaped PET substrates that have poor oxygen permeability. The transparent and stretchable characteristics of the graphene–AgNW hybrid electrodes can provide good electrical interfaces between the rigid ILED and deformable, soft contact lens substrate. The fabrication process began with the CVD synthesis of graphene on a Cu foil. After coating AgNW networks on the graphene surface, another graphene passivation layer covered the NWs to prevent the possible loss of the NWs by tears. Patterning the hybrid nanostructure using oxygen plasma followed by etching the Cu foil and then transferring the hybrid electrode onto a soft contact lens (soft galyfilcon A polymer). Placing light-emitting diodes (RazerThin RT290, Cree, Inc.) on the top surface of the electrodes using a tweezer completed the fabrication step. Figure 4a and b shows a schematic diagram of the device layouts and photographs of this sample. The contact lens area under the ILED (dimension: 270 μm × 270 μm × 95 μm) becomes sunk down slightly due to the ILED weight (inset of Figure 4b). The superb flexibility and stretchability of this hybrid electrode enable its planar layout to be wrapped on the curved, hemispherical outside surface of the contact lens comfortably. Figure 4c presents the ILED sample worn on the eye of a mannequin, and this device can operate to emit light by supplying bias of 4 V (Supporting Movie 1). As an *in vivo* study, this contact lens was worn by a live rabbit eye for five hours (Figure 4d), and we have not observed any abnormal behavior of the live rabbit (Female New Zealand White Rabbit), such as bloodshot eyes or the rubbing of eye areas. Supporting Movie 2 shows the movement of the rabbit with wearing the contact lens device. After wearing for five hours, the contact lens was removed from the ocular surface to measure the current–voltage characteristics of the device using a probe station. As shown in Figure 4e, the ILED on the contact lens is still working with emitting light. The turn-on voltage is maintained after this *in vivo* experiment, but resistance is increased (i.e., slope is lowered) due to the slight slipping of ILED on the surface of the hybrid electrode by the regular eye nictation of the live rabbit. The developments of biocompatible and conductive adhesives, fabrications of multiple pixel displays on wearable contact lenses, and integrations of antennas for wireless power transmission represent next steps toward the future displays.

The graphene–AgNW hybrid electrode can be used as source/drain of oxide semiconductor thin film transistors (TFTs). For this demonstration, an In–Ga–Zn–O (IGZO) semiconducting layer (thickness: 50 nm) was sputtered on a Si wafer with a SiO_2 dielectric top surface (thickness: 75 nm), and then stripe patterns of IGZO were formed using wet etching process. Transferring source/drain electrodes of the hybrid onto this IGZO layer using the same procedures described above completed the fabrication of TFTs. Figure 5a presents a schematic diagram of this transistor layout. The channel length and width of the TFT are 100 μm, as shown in Figure 5b. Figure 5c and d presents the transfer and full output characteristics of the IGZO TFTs, respectively. The graphs indicate typical n-channel behavior. The TFT performance was measured with the mobility of 8.2 $cm^2/V{\cdot}s$ in the linear regime (or 6.1 $cm^2/V{\cdot}s$ in the saturation regime) and on/off ratio of $\sim 10^6$. In contrast to single materials of AgNWs or graphene, the improved robustness of the graphene–AgNW hybrid that can withstand electrical load enables stable TFT operations without the breakdown of source/drain electrodes. The mobility of this TFT is slightly lower than typical mobilities of IGZO TFT with Al source/drains ($\sim$10 $cm^2/V{\cdot}s$ in the linear regime), potentially due to high contact resistances. However, the mobility of this TFT with the hybrid electrodes is still higher than mobilities of the amorphous Si TFTs ($\sim$1 $cm^2/V{\cdot}s$) that are mainly used for commercial LCD or OLED displays. Also, high transparency and flexibility of the hybrid

dx.doi.org/10.1021/nl401070p | *Nano Lett.* 2013, 13, 2814−2821

electrode are advantageous for transparent and flexible TFT arrays, and this process is currently underway.

In conclusion, the work presented here demonstrates the advantages of graphene−AgNW hybrid nanostructures as flexible and stretchable, transparent electrodes. Integration of two-dimensional graphene and one-dimensional NWs in a hybrid film could significantly enhance electrical properties such as low R_s and strong robustness against electrical breakdown, with negligible degradation of optical transmittance. The graphene layer which covers AgNWs reliably preserves these properties against thermal oxidation. Also, the hybrid electrode presents superb mechanical flexibility and stretchability that enables complete folding in half. Fabrications of oxide semiconductor transistors and single-pixel displays on wearable, soft eye contact lenses with in vivo studies provide examples of the use of the hybrid electrodes. We believe the hybridization between two-dimensional and one-dimensional nanomaterials presents a promising strategy toward flexible, wearable electronics and implantable biosensor devices and indicates the substantial promise of future electronics.

■ ASSOCIATED CONTENT

Ⓢ Supporting Information

Experimental details of CVD graphene synthesis, AgNW coating, transfer of the hybrid structures, device fabrications, and supporting figures and movies. This material is available free of charge via the Internet at http://pubs.acs.org.

■ AUTHOR INFORMATION

Corresponding Author

*E-mail: jangung@unist.ac.kr.

Notes

The authors declare no competing financial interest.

■ ACKNOWLEDGMENTS

The authors thank Prof. Sung Jun Kang for ILED support. This work was supported by the National Research Foundation of Korea (20110014111) and the Ministry of Knowledge Economy through the Materials Original Technology Program (10041222), IT R&D program (10041416), and New & Renewable Energy Technology Development Program (20113020010060). J.-U.P. thanks UNIST and Samsung Display for financial support through the 2012 Research Fund (1.120001.01).

■ REFERENCES

(1) Burroughes, J. H.; Bradley, D. D. C.; Brown, A. R.; Marks, R. N.; Mackay, K.; Friend, R. H.; Burns, P. L.; Holmes, A. B. Light-Emitting Diodes Based on Conjugated Polymers. *Nature* **1990**, *347*, 539−541.

(2) Yu, G.; Cao, A.; Lieber, C. M. Large-area Blown Bubble Films of Aligned Nanowires and Carbon Nanotubes. *Nat. Nanotechnol.* **2007**, *2*, 372−377.

(3) Park, J.-U.; Meitl, M. A.; Hur, S.-H.; Usrey, M. L.; Strano, M. S.; Kenis, P. J. A.; Rogers, J. A. In-situ Deposition and Patterning of Single-Walled Carbon Nanotubes By Laminar Flow and Controlled Flocculation in Microfluidic Channels. *Angew. Chem., Int. Ed.* **2006**, *45*, 581−585.

(4) Wu, Z.; Chen, Z.; Du, X.; Logan, M. J.; Sippel, J.; Nikolou, M.; Karamas, K.; Reynolds, J. R.; Tanner, D. B.; Hebard, A. F.; et al. Transparent, Conductive Carbon Nanotube Films. *Science* **2004**, *305*, 1273−1276.

(5) Shim, B. S.; Zhu, J. A.; Jan, E.; Critchley, K.; Kotov, N. A. Transparent Conductors form Layer-by-Layer Assembled SWNT Films: Importance of Mechanical Properties and a New Figure of Merit. *ACS Nano* **2010**, *4*, 3725−3734.

(6) Park, J.-U.; Nam, S.; Lee, M.-S.; Lieber, C. M. Synthesis of Monolithic Graphene-Graphite Integrated Electronics. *Nat. Mater.* **2012**, *11*, 120−125.

(7) Nair, R. R.; Blake, P.; Grigorenko, A. N.; Novoselov, K. S.; Booth, T. J.; Stauber, T.; Peres, N. M. R.; Geim, A. K. Fine Structure Constant Defines Visual Transparency of Graphene. *Science* **2008**, *320*, 1308.

(8) Chen, J.-H.; Jang, C.; Xiao, S.; Ishigami, M.; Fuhrer, M. S. Intrinsic and Extrinsic Performance Limits of Graphene Devices on SiO_2. *Nat. Nanotechnol.* **2008**, *3*, 206−209.

(9) Emtsev, K. V.; Bostwick, A.; Horn, K.; Jobst, J.; Kellogg, G. L.; Ley, L.; McChesney, J. L.; Ohta, T.; Reshanov, S. A.; Rohrl, J. Towards Wafer-size Graphene Layers by Atmospheric Pressure Graphitization of Silicon Carbide. *Nat. Mater.* **2009**, *8*, 203−207.

(10) Reina, A.; Jia, X.; Ho, J.; Nezich, D.; Son, H.; Bulovic, V.; Dresselhaus, M. S.; Kong, J. Large Area, Few-Layer Graphene Films on Arbitrary Substrates by Chemical Vapor Deposition. *Nano Lett.* **2008**, *9*, 30−35.

(11) Li, X.; Cai, W.; An, J.; Kim, S.; Nah, J.; Yang, D.; Piner, R.; Velamakanni, A.; Jung, I.; Tutuc, E. Large-Area Synthesis of High-Quality and Uniform Graphene Films on Copper Foils. *Science* **2009**, *324*, 1312−1314.

(12) Kim, K. S.; Zhao, Y.; Jang, H.; Lee, S. Y.; Kim, J. M.; Kim, K. S.; Ahn, J. H.; Kim, P.; Choi, J. Y.; Hong, B. H. Large-Scale Pattern Growth of Graphene Films for Stretchable Transparent Electrodes. *Nature* **2009**, *457*, 706−710.

(13) Li, X. S.; Zhu, Y. W.; Cai, W. W.; Borysiak, M.; Han, B. Y.; Chen, D.; Piner, R. D.; Colombo, L.; Ruoff, R. S. *Nano Lett.* **2009**, *9*, 4359−4363.

(14) Bae, S.; Kim, H.; Lee, Y.; Xu, X.; Park, J.-S.; Zheng, Y.; Balakrishnan, J.; Lei, T.; Kim, H. R.; Song, Y. I.; Kim, Y.-J.; Kim, K. S.; Özyilmaz, B.; Ahn, J.-H.; Hong, B. H.; Iijima, S. Roll-to-Roll Production of 30 in. Graphene Films for Transparent Electrodes. *Nat. Nanotechnol.* **2010**, *5*, 574−578.

(15) Zhu, Y.; Sun, Z.; Yan, Z.; Jin, Z.; Tour, J. M. Rational Design of Hybrid Graphene Films for High-Performance Transparent Electrodes. *ACS Nano* **2011**, *5*, 6472−6479.

(16) Kim, K. K.; Reina, A.; Shi, Y.; Park, H.; Li, L.-J.; Lee, Y. H.; Kong, J. Enhancing the Conductivity of Transparent Graphene Films via Doping. *Nanotechnology* **2010**, *21*, 285205.

(17) Lieber, C. M. Semiconductor Nanowires: A Platform for Nanoscience and Nanotechnology. *MRS Bull.* **2011**, *36*, 1052−1063.

(18) Wang, C.; Hu, Y.; Lieber, C. M.; Sun, S. Ultrathin Au Nanowires and Their Transport Properties. *J. Am. Chem. Soc.* **2008**, *130*, 8902−8903.

(19) Wu, Y.; Xiang, J.; Yang, C.; Lu, W.; Lieber, C. M. Single-crystal Metallic Nanowires and Metal/semiconductor Nanowire Heterostructures. *Nature* **2004**, *430*, 61−65.

(20) Wang, D.; Lieber, C. M. Inorganic Materials; Nanocrystals Branch Out. *Nat. Mater.* **2003**, *2*, 355−356.

(21) De, S.; Higgins, T. M.; Lyons, P. E.; Doherty, E. M.; Nirmalraj, P. N.; Blau, W. J.; Boland, J. J.; Coleman, J. N. Silver Nanowire Networks as Flexible, Transparent, Conducting Films: Extremely High DC to Optical Conductive Ratios. *ACS Nano* **2009**, *3*, 1767−1774.

(22) Hu, L.; Kim, H. S.; Lee, J.-Y.; Peumans, P.; Cui, Y. Scalable Coating and Properties of Transparent, Flexible, Silver Nanowire Electrodes. *ACS Nano* **2010**, *4*, 2955−2963.

(23) De, S.; Coleman, J. N. The Effects of Percolation in Nanostructured Transparent Conductors. *MRS Bull.* **2011**, *36*, 774−781.

(24) Yang, L.; Zhang, T.; Zhou, H.; Price, S. C.; Wiley, B. J.; You, W. Solution-Processed Flexible Polymer Solar Cells with Silver Nanowire Electrodes. *ACS Appl. Mater. Interfaces* **2011**, *3*, 4075−4084.

(25) Hu, W.; Niu, X.; Li, L.; Yun, S.; Yu, Z.; Pei, Q. Intrinsically Stretchable Transparent Electrodes Based on Silver-Nanowire-Cross-linked-Polyacrylate Composites. *Nanotechnology* **2012**, *23*, 344002.

(26) Hu, L.; Wu, H.; Cui, Y. Metal Nanogrids, Nanowires, and Nanofibers for Transparent Electrodes. *MRS Bull.* **2011**, *36*, 760−765.

(27) Catrysse, P. B.; Fan, S. H. Nanopatterned Metallic Films for Use As Transparent Conductive Electrodes in Optoelectronic Devices. *Nano Lett.* **2010**, *10*, 2944−2949.
(28) Ahn, S. H.; Guo, L. J. Spontaneous Formation of Periodic Nanostructures by Localized Dynamic Wrinkling. *Nano Lett.* **2010**, *10*, 4228−4234.
(29) Jeong, C.; Nair, P.; Khan, M.; Lundstrom, M.; Alam, M. A. Prospects for Nanowire-Doped Polycrystalline Graphene Films for Ultratransparent, High Conductive Electrodes. *Nano Lett.* **2011**, *11*, 5020−5025.
(30) Kholmanov, I. N.; Stoller, M. D.; Edgeworth, J.; Lee, W. H.; Li, H.; Lee, J.; Barnhart, C.; Potts, J. R.; Piner, R.; Akinwande, D.; Barrick, J. E.; Ruoff, R. S. Nanostructured Hybrid Transparent Conductive Films with Antibacterial Properties. *ACS Nano* **2012**, *6*, 5157−5163.
(31) Kholmanov, I. N.; Magnuson, C. W.; Aliev, A. E.; Li, H.; Zhang, B.; Suk, J. W.; Zhang, L. L.; Peng, E.; Mousavi, S. H.; Khanikaev, A. B.; Piner, R.; Shvets, G.; Ruoff, R. S. Improved Electrical Conductivity of Graphene Films Integrated with Metal Nanowires. *Nano Lett.* **2012**, *12*, 5679−5683.
(32) Zhao, J.; Sun, H.; Dai, S.; Wang, Y.; Zhu, J. Electrical Breakdown of Nanowires. *Nano Lett.* **2011**, *11*, 4647−4651.
(33) Kang, C. G.; Lee, S. K.; Lee, Y. G.; Hwang, H. J.; Cho, C.; Lim, S. K.; Heo, J.; Chung, H.-J.; Yang, H.; Seo, S.; Lee, B. H. Enhanced Current Drivability of CVD graphene Interconnect in Oxygen-Deficient Environment. *IEEE Electron Device Lett.* **2011**, *32*, 1591−1593.
(34) Lee, C.; Wei, X.; Kysar, J. W.; Hone, J. Measurement of the Elastic Properties and Intrinsic Strength of Monolayer Graphene. *Science* **2008**, *321*, 385−388.
(35) Kim, D.-H.; Rogers, J. A. Stretchable Electronics: Materials Strategies and Devices. *Adv. Mater.* **2008**, *20*, 4887−4892.
(36) Bunch, S.; Verbridge, S. S.; Alden, J. S.; van der Zande, A. M.; Parpia, J. M.; Craighead, H. G.; McEuen, P. L. Impermeable Atomic Membranes from Graphene Sheets. *Nano Lett.* **2008**, *8*, 2458−2462.
(37) Chen, S.; Brown, L.; Levendorf, M.; Cai, W.; Ju, S.; Edgeworth, J.; Li, X.; Magnuson, C. W.; Velamakanni, A.; Piner, R. D.; Kang, J.; Park, J.; Ruoff, R. S. Oxidation Resistance of Graphene-Coated Cu and Cu/Ni Alloy. *ACS Nano* **2011**, *5*, 1321−1327.
(38) Lingley, A. R.; Ali, M.; Liao, Y.; Mirjalili, R.; Klonner, M.; Sopanen, M.; Suihkonen, S.; Shen, T.; Otis, B. P.; Lipsanen, H.; Parviz, B. A. A Single-Pixel Wireless Contact Lens Display. *J. Micromech. Microeng.* **2011**, *21*, 125014.
(39) Stauth, S. A.; Parviz, B. A. Self-Assembled Single-crystal Silicon Circuits on Plastic. *Proc. Natl Acad. Sci.* **2006**, *103*, 13922−7.
(40) Parviz, B. A. For Your Eye Only. *IEEE Spectrum* **2009**, *46*, 36−41.